Biomass estimation from simulated GEDI, ICESat-2 and NISAR across environmental gradients in Sonoma County, California

Remote Sensing of Environment 242 (2020) 111779

Contents lists available at ScienceDirect

Remote Sensing of Environment

journal homepage: www.elsevier.com/locate/rse

Biomass estimation from simulated GEDI, ICESat-2 and NISAR across environmental gradients in Sonoma County, California

Laura Duncanson[a,b,*], Amy Neuenschwander[c], Steven Hancock[a,d], Nathan Thomas[b,e], Temilola Fatoyinbo[b], Marc Simard[f], Carlos A. Silva[a], John Armston[a], Scott B. Luthcke[g], Michelle Hofton[a], James R. Kellner[h,i], Ralph Dubayah[a]

[a] Department of Geographical Sciences, University of Maryland, College Park, USA
[b] Biospheric Sciences Lab, NASA Goddard Space Flight Center, USA
[c] Applied Research Laboratories, University of Texas at Austin, USA
[d] School of GeoSciences, University of Edinburgh, United Kingdom of Great Britain and Northern Ireland
[e] Earth System Science Interdisciplinary Center, University of Maryland, College Park, USA
[f] Radar Science and Engineering Section, NASA Jet Propulsion Laboratory, USA
[g] Geodesy and Geophysics Lab, NASA Goddard Space Flight Center, USA
[h] Department of Ecology and Evolutionary Biology, Brown University, USA
[i] Institute at Brown for Environment and Society, Brown University, USA

ARTICLE INFO

Edited by Jing M. Chen

Keywords:
GEDI
NISAR
ICESat-2
Biomass estimation
Biomass errors
Data fusion

ABSTRACT

Estimates of the magnitude and distribution of aboveground carbon in Earth's forests remain uncertain, yet knowledge of forest carbon content at a global scale is critical for forest management in support of climate mitigation. In light of this knowledge gap, several upcoming spaceborne missions aim to map forest aboveground biomass, and many new biomass products are expected from these datasets. As these new missions host different technologies, each with relative strengths and weaknesses for biomass retrieval, as well as different spatial resolutions, consistently comparing or combining biomass estimates from these new datasets will be challenging. This paper presents a demonstration of an inter-comparison of biomass estimates from simulations of three NASA missions (GEDI, ICESat-2 and NISAR) over Sonoma county in California, USA. We use a high resolution, locally calibrated airborne lidar map as our reference dataset, and emphasize the importance of considering uncertainties in both reference maps and spaceborne estimates when conducting biomass product validation. GEDI and ICESat-2 were simulated from airborne lidar point clouds, while UAVSAR's L-band backscatter was used as a proxy for NISAR. To estimate biomass for the lidar missions we used GEDI's footprint-level biomass algorithms, and also adapted these for application to ICESat-2. For UAVSAR, we developed a locally trained biomass model, calibrated against the ALS reference map. Each mission simulation was evaluated in comparison to the local reference map at its native product resolution (25 m, 100 m transect, and 1 ha) yielding RMSEs of 57%, 75%, and 89% for GEDI, NISAR, and ICESat-2 respectively. RMSE values increased for GEDI's power beam during simulated daytime conditions (64%), coverage beam during nighttime conditions (72%), and coverage beam daytime conditions (87%). We also test the application of GEDI's biomass modeling framework for estimation of biomass from ICESat-2, and find that ICESat-2 yields reasonable biomass estimates, particularly in relatively short, open canopies. Results suggest that while all three missions will produce datasets useful for biomass mapping, tall, dense canopies such as those found in Sonoma County present the greatest challenges for all three missions, while steep slopes also prove challenging for single-date SAR-based biomass retrievals. Our methods provide guidance for the inter-comparison and validation of spaceborne biomass estimates through the use of airborne lidar reference maps, and could be repeated with on-orbit estimates in any area with high quality field plot and ALS data. These methods allow for regional interpretations and filtering of multi-mission biomass estimates toward improved wall-to-wall biomass maps through data fusion.

* Corresponding author at: 2181 Lefrak Hall, University of Maryland, College Park, MD, USA.
E-mail address: lduncans@umd.edu (L. Duncanson).

https://doi.org/10.1016/j.rse.2020.111779
Received 14 November 2019; Received in revised form 10 March 2020; Accepted 13 March 2020
Available online 01 April 2020

1. Introduction

1.1. Background on biomass modeling/mapping

The accurate estimation of terrestrial forest biomass is crucial for understanding the role of forests in the global carbon cycle. The total forest carbon reservoir (including below ground carbon) is equivalent to about 85% of terrestrial stocks and 75% of terrestrial gross primary production (Pan et al., 2013), yet estimates of the distribution and flux of carbon in Earth's forests remain highly uncertain, with current global biomass and vegetation structure estimates being too coarse for many science and policy applications (Hall et al., 2011; Houghton et al., 2012). Further, estimates of carbon emissions from land use change associated with forest conversion result in large mismatches between mean global carbon uptake and atmospheric CO_2 growth rates of up to 10 Pg C year $^{-1}$ (Zscheischler et al., 2017) depending on whether the land sink estimation is bottom-up, i.e. based on long term, ground data (Pan et al., 2011, 2013) or top-down, meaning that it is the residual of the increase in atmospheric carbon and the net ocean carbon flux (Le Quéré et al., 2017).

Remote sensing-based biomass estimates are key to improving bottom-up carbon flux estimates, as these incorporate both changes in forest extent and biomass density. Similarly, the implementation of national greenhouse gas (GHG) emission inventories and Payment for Ecosystem services (PES) schemes such as REDD+ depends on the development of Monitoring, Reporting, Verification (MRV) guidelines that are based on knowledge of the extent, carbon density and change of forested areas. The anticipation of PES through REDD+, and the need to reduce the uncertainties around the global land sink, have resulted in an increased number of studies on the spatial distribution of aboveground biomass and carbon stocks in forest ecosystems, such as from global pantropical biomass maps (Baccini et al., 2012; Blair and Hofton, 1999; Saatchi et al., 2011).

A new generation of active remote sensing technologies will largely fill the need for new global estimates of aboveground biomass. This paper focuses on three new missions, NASA's Global Ecosystem Dynamics Investigation (GEDI), NASA's Ice Cloud and land Elevation Satellite (ICESat-2), and the NASA-Indian Space Research Organization (ISRO) Synthetic Aperture Radar (NISAR). We simulate these three mission datasets with the aim of demonstrating methods for biomass estimate intercomparison from three different data streams each with its own strengths and limitations for forest structure mapping.

While each of these three missions (NISAR, GEDI and ICESat-2) will make forest canopy observations that may be used to estimate vegetation biomass, the signals returned from vegetated surfaces will be influenced by topography and forest structure. The missions with vegetation structure requirements (GEDI and NISAR) have carefully evaluated these issues in a variety of landscapes, both from theoretical and applied perspectives (NISAR handbook, Dubayah et al., 2020). The impacts of surface structural complexity for ICESat-2, conversely, are relatively unknown in temperate systems given the lack of a vegetation product requirement by the ICESat-2 mission. Scientists on each mission team have predicted the expected performance of the missions for biomass (Neuenschwander and Magruder, 2016; Yu and Saatchi, 2016), but no assessment has been conducted exploring potential utility at a single site for all three missions. Fusing SAR and lidar datasets over forested areas and developing new algorithms that incorporate the benefits of each dataset may improve our ability to estimate forest biomass with higher accuracies and at spatial resolutions appropriate for land management.

A consistent exploration of the biomass estimation limitations of these upcoming datasets will help inform the development of fusion techniques, particularly in structurally complex environments (e.g. high biomass mixed forests in mountainous areas). It is well accepted that errors increase with increasing biomass densities, both due to a) increased natural structural variability in mature, higher biomass forests systems, b) increased edge effects, particularly in areas with wider tree crowns, and c) increased errors associated with the application of allometric models (Réjou-Méchain et al., 2019). Therefore a deviation in, say, a GEDI biomass estimate from a reference pixel biomass estimate in a mature, high biomass area may well be within the wider confidence limits of the reference map in that area as compared to a tighter confidence interval in a lower biomass forest. Thus, all airborne lidar reference maps have limitations in their utility as reference datasets.

The goals of this study are three-fold. First, to demonstrate methods for validation of satellite-based biomass estimates through comparison to a locally calibrated airborne lidar biomass map. Second, to determine trends in relationships between biomass estimation error and environment for GEDI, ICESat-2 and NISAR in a particularly challenging high biomass domain, and third, to test the application of GEDI's biomass algorithms on ICESat-2 data.

1.2. SAR and lidar mission status

1.2.1. GEDI

The GEDI mission is the first spaceborne lidar designed specifically to study forest structure (Dubayah, 2020; Dubayah et al., 2020). GEDI is a NASA Earth Venture Instrument (EVI) that was selected in 2014, and implements a 3-laser, full waveform recording Lidar instrument operating from the Japanese Experimental Module's Exposed Facility (JEM-EF) on the International Space Station (ISS). GEDI launched on December 5, 2018, and will operate for a nominal 2-year minimum period, producing ~10 billion cloud-free land surface observations. GEDI's 3 lasers operate at 1064 nm, while one laser is split into two weaker energy beams, resulting in four GEDI beams, each illuminating footprints (areas on the Earth's surface from which Lidar energy is reflected) with a ~25 m diameter. These beams are optically dithered to produce eight ground tracks with approximately 60 m along track sampling returning full waveform lidar observations with a 2–3 cm vertical measurement accuracy. GEDI full waveform along track observations are acquired from 8 tracks spaced 600 m apart effectively sampling data from a 4.2 km wide swath. The GEDI instrument has the ability to point or roll about an axis approximately aligned with the ISS velocity vector. Therefore, the instrument pointing enables optimal sampling such that the center of the GEDI swath follows a set of pre-defined Reference Ground Tracks (RGTs) even though the ISS is not in a repeating orbit. The RGTs are computed to be as congruent with the ISS orbit as possible, facilitating minimal instrument off-pointing, therefore at the same 51.6° inclination as the ISS orbit.

For each footprint, GEDI will have a suite of waveform metrics, including canopy height and relative height (RH) metrics, canopy profile metrics, and ground elevation. These waveform metrics are also used to estimate aboveground biomass density (AGBD) using empirically derived calibration models. GEDI footprint-level biomass estimates will then be gridded to 1 km products, although as aforementioned GEDI's gridding algorithm is not assessed in this paper. The GEDI Science Definition Team (SDT) has compiled a global database of coincident in situ field and airborne lidar datasets to develop the footprint-level calibration models which will convert GEDI metrics to biomass. In this process, airborne lidar data are used to simulate GEDI waveforms (Hancock et al., 2019), and these waveforms are used to train the biomass calibration models that are applied to the on-orbit GEDI data.

1.2.2. NISAR

NISAR is a multi-disciplinary mission born from a joint partnership between NASA and the Indian Space Research Organization (ISRO), and its platform will host both L-band (24 cm wavelength) and S-band (10 cm wavelength) radars. NISAR will collect data with a spatial resolution of 7 m over a swath width ~242 km using a 12 m diameter deployable mesh reflector (NISAR User Handbook). NISAR is scheduled to launch at the end of 2021 for a minimum 3-year mission with

capacity for extended operations. The satellite will be in a 12-day repeat orbit at an altitude of 740 km (Rosen et al., 2016). The mission will therefore achieve global coverage every 6 days considering both ascending and descending orbital passes. The current mission plan is for co-polarization mode (HH) acquisitions every 6-days, and cross-polarization mode (HV) acquisitions three times every 24 days. This results in each location on Earth being imaged ~60 times each year.

The NISAR L-band radar backscatter measurements will enable the generation of an annual global biomass map with a spatial scale of 1 ha. The mission is required to cover at least 80% of forested areas with biomass ≤100 Mg/ha and with no > 20% error. Forest disturbance and recovery will also be monitored annually at the 1 ha resolution (Yu and Saatchi, 2016). The radar measurements will provide these biomass estimates irrespective of illumination and atmospheric conditions and will not be perturbed by cloud cover which is prominent in the tropics.

1.2.3. ICESat-2

The ICESat-2 satellite was launched on September 15, 2018, and provides a global distribution of geodetic measurements from a space-based laser altimeter of both the ground and canopy surfaces. The primary science objective of these measurements over land is the estimation of vegetation canopy height which will also enable height-based biomass estimation. The Advanced Topographic Laser Altimeter System (ATLAS) instrument on-board ICESat-2 is a photon counting laser altimeter. ICESat-2 generates two geophysical data products specifically focused on land and vegetation: ATL08, the Level 3 along-track data product and ATL18, the Level 4 gridded product. ATL08 will report terrain height estimates, canopy height estimates, and relative height metrics such as: RH25, RH50, RH60, RH70, RH75, RH80, RH85, RH90, and RH98 at a 100 m step.

ATLAS operates at 532 nm in the green range of the electromagnetic (EM) spectrum and fires at a rate of 10 kHz. The combination of the laser repetition rate and satellite velocity will result in one outgoing laser pulse approximately every 70 cm on the Earth's surface and each spot on the surface is ~13 m in diameter (Magruder et al., 2020). Over vegetation, the number of detected, returned photons from each outgoing laser pulse is expected to range between 0 and 4 photons, depending upon canopy cover, atmospheric transmission, and surface reflectance (Neuenschwander and Pitts, 2019). That detection can occur anywhere within the vertical distribution of the reflected signal, that is, anywhere within the vertical distribution of the canopy. This uncertainty of where the photon will be returned is referred to as the vertical sampling error (Neuenschwander and Magruder, 2016). The photon-counting technology has many advantages for space-based altimetry but also has challenges, particularly with delineating signal from background noise. Simulation studies to estimate vertical sampling error indicate that the canopy heights reported on the ATL08 data product will underestimate the top canopy height in the range of 1–4 m at its 100-m transect resolution (Neuenschwander and Magruder, 2016). Due to the high laser pulse repetition rate and smaller footprint size, the along-track point density is relatively high and the ICESat-2 algorithms have been written to separate vegetation returns from ground returns, even in areas of high relief – an improvement from ICESat/GLAS where the topographic signal was convolved with the vegetation signal in areas with relief > 10% (Chen, 2010; Duncanson et al., 2010; Hilbert and Schmullius, 2012; Neuenschwander and Pitts, 2019).

1.2.4. Mission biomass requirements

The GEDI and NISAR missions both have formal requirements for generating data to enable the production of biomass maps, while ICESat-2 has no formal biomass requirement. GEDI's science requirements are to measure forest height and vertical structure at the footprint (~25 m) resolution, and to estimate biomass at the specified grid resolution of 1 km with an uncertainty of 20% Standard Error (SE) or better in 80% of the GEDI domain 1 km cells. The NISAR mission is required to enable estimates of biomass annually with a spatial resolution of 1 ha, with an accuracy of 20 Mg/ha (RMSE) in at least 80% of forest areas with biomass below 100 Mg/ha. GEDI and ICESat-2, as sampling missions, will have gaps across tracks, and also from clouds, while NISAR will provide wall-to-wall data. GEDI is designed to provide data for measuring forest structure across all ranges of biomass up to ~99.8% canopy cover, while NISAR's requirements are limited to biomass values below 100 Mg/ha (up to ~70% canopy cover in Sonoma County). ICESat-2 is expected to provide estimates for a range of biomass between GEDI and NISAR, limited mainly by its ability to penetrate canopy cover, although this limit has not yet been established. Because of the ISS orbit, GEDI will only collect data under the ISS orbit, between 51.6° North and South, while both ICESat-2 and NISAR provide global coverage. Native footprint sizes are about 25 m for GEDI and 3 m × 8 m slant range resolution for NISAR. ICESat-2 collects approximately 0–4 photons from each ~13 m footprint over vegetated surfaces, but densely overlapping footprints (spaced 70 cm along track) provide canopy height transects with a length of about 100 m and width of ~13 m. Thus, in this paper we focus on estimating biomass not at the expected mission gridded product resolutions, but at the resolution of the finest biomass estimates expected from each mission (i.e. 25 m diameter circles for GEDI, 100 m transects for ICESat-2, and in this case an aggregated 1 ha resolution for NISAR, although the measurement units for NISAR are higher resolution). Table 1 provides a summary of the three missions addressed in this study, including the expected gridded mission biomass products in comparison to the scale at which we conduct our analyses using simulated mission datasets.

2. Methods

This study presents a comparison of biomass estimates from simulated spaceborne datasets to a local reference biomass map, and calculates multiple statistics for each spaceborne estimate. To help guide the reader in the interpretation of our results, for the remainder of the paper we use the following definitions: Uncertainty is defined as the 90th percentile confidence interval around a prediction of aboveground biomass density, both for reference pixels and simulated spaceborne estimates. In this paper we define error as the deviation between a biomass estimate and its true value, which again we assume here to be its airborne lidar reference value. A more accurate estimate will have a

Table 1
Summary of key mission specifications and resolutions.

	ICESat-2	GEDI	NISAR
Launch date	September 15, 2018	December 5, 2018	2022
Wavelength	532 nm (green)	1064 nm (near IR)	S&L band
Geographic coverage	Global	ISS: ± ~ 51.6°	Global
Measurement strategy	6 tracks from 1 laser (3 power tracks)	8 tracks from 3 lasers (4 power tracks, 4 coverage tracks)	Wall-to-wall
Native measurement resolution	~13 m footprints returning 0–4 photons	~25 m footprints returning full waveforms	3 m × 8 m slant range resolution
Biomass product resolution(s)	NA	25 m footprint estimates; 1 km gridded estimates	1 ha
Resolution tested in this study	100 m along track transects	25 m circular footprint	1 ha

lower deviation between the estimate and the reference value. The Root Mean Squared Error (RMSE) then is defined as the square root of the mean of the squared deviations between simulated spaceborne pixel estimates and airborne lidar reference map estimates. We concede that this is technically incorrect, as residuals by definition are deviations between estimates and observations, but observations of forest AGBD are not available in the vast majority of field or lidar studies, and typically rely on the application of allometric models as we have done here (Clark and Kellner, 2012).

2.1. Study area

This study was conducted in Sonoma County, California, where airborne proxies for all three missions (GEDI, NISAR and ICESat-2) are available. The majority of Sonoma County is classified as either conifer forest, grassland, or shrubland, with large portions of developed areas, mixed forests, and cropland (Homer et al., 2015). In terms of biomass composition, more than half of the modeled biomass in Sonoma County falls in pixels classified as conifer forests, followed by scrubland and mixed forest. Fig. 2 shows the distribution of biomass, percent canopy cover, slope, and forest height across the study area. The study area spans wide variety of elevation, slope, tree height, canopy cover and biomass, thus enabling an analysis of anticipated mission data strengths and limitations in different forest conditions.

2.2. Data

2.2.1. Sonoma ALS and biomass map

Wall-to-wall ALS were collected over Sonoma County in the fall of 2013 using Leica ALS50 and ALS70 instruments giving coverage over the whole county at 14 points m^{-2} (Dubayah et al., 2013). These data were used to generate a 30 m biomass map for all of Sonoma County (Dubayah et al., 2013) using a random forest model and calibrated with 166 field plots collected at a random sample of locations stratified by land cover type (Duncanson et al., 2017; Huang et al., 2017). These field plots largely missed the highest biomass areas of Sonoma County, and the maximum biomass density was ~500 Mg/ha, thus the random forest model set all high biomass redwood forests to this maximum value. A new reference map was regenerated, using 30 additional plots sampled in redwood forests across the county using an Ordinary Least Squares (OLS) modeling approach (SI Fig. 1), and the variance covariance matrix from this model was sampled to produce 1000 estimates for every 30 m pixel across Sonoma County. 90th percentile confidence intervals were calculated from the 1000 sets of predicted biomass for each pixel, and as expected we find wider confidence intervals in higher biomass forests (Fig. 1). Developed areas were masked from this analysis using a high resolution forest non-forest mask described in (Dubayah et al., 2013).

2.2.2. GEDI simulations

ALS data were processed to simulate GEDI waveforms across the entire county representing two years of on-orbit performance (Fig. 3). The GEDI simulator is described in detail and validated in Hancock et al. (2019). Waveforms are simulated following the methods proposed in (Blair and Hofton, 1999), and white Gaussian noise is added (Hancock et al., 2011) to provide the same signal-to-noise ratio (SNR) predicted by pre-launch analysis of the instrument performance for mean atmospheric transmission, solar background illumination and the expected detector response (Davidson and Sun, 1988). This allows GEDI-like signals to be generated from any ALS data, with simulations

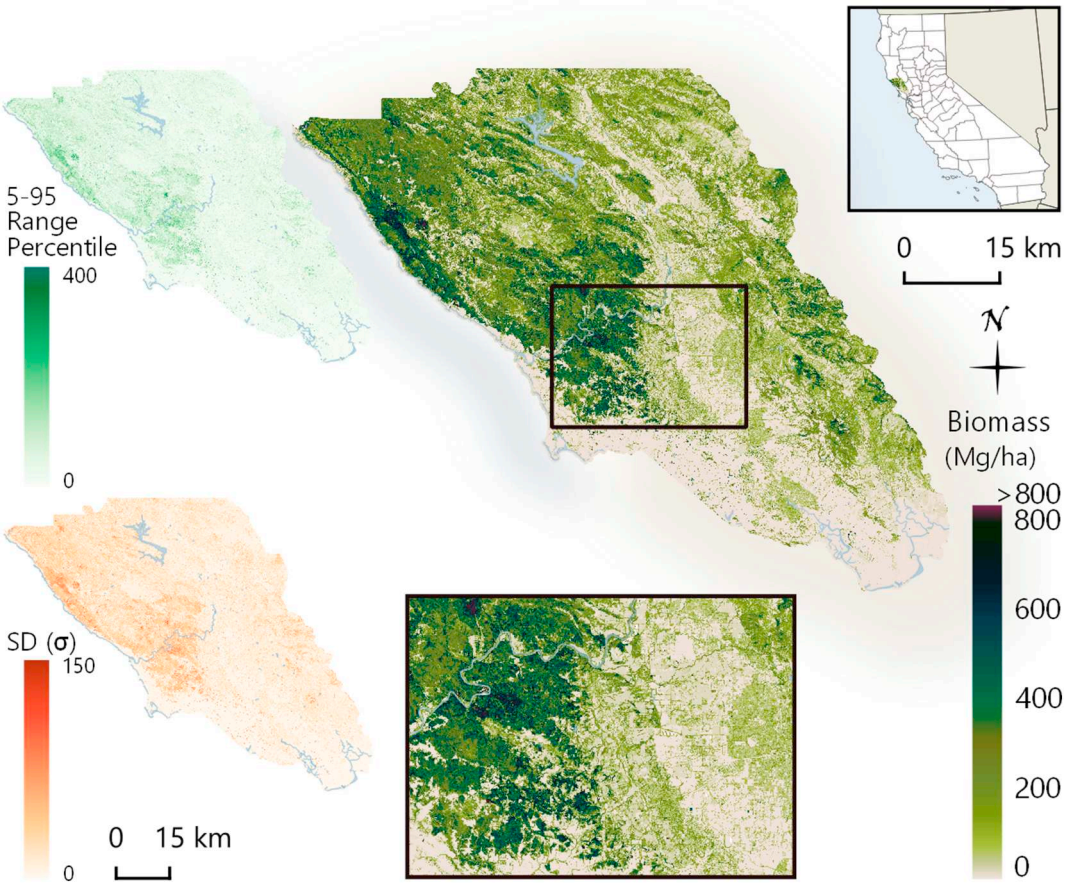

Fig. 1. A Sonoma County-wide 30 m ALS biomass map was used as the biomass reference map for this study. The 90th percentile and standard deviations of biomass from a model bootstrapping are shown on the left.

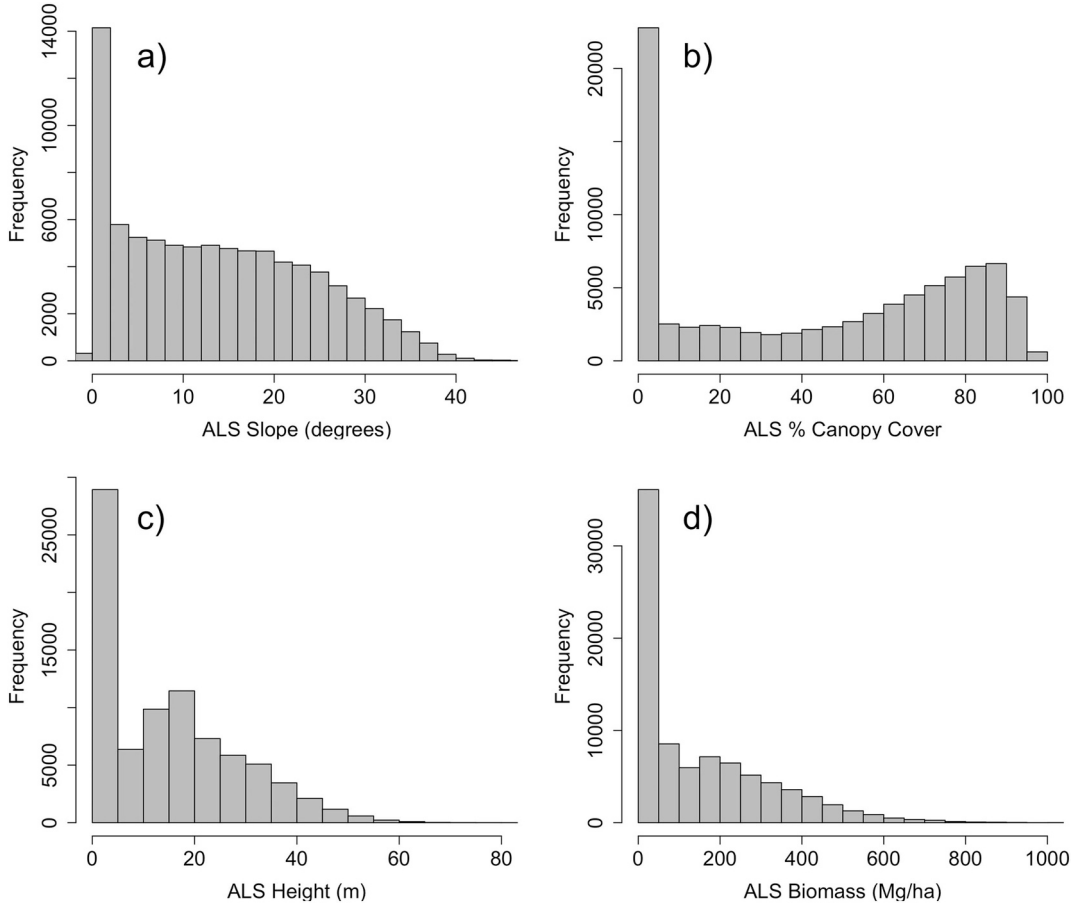

Fig. 2. Histograms of ALS-derived (a) slope, (b) % canopy cover (b), (c) height and (d) biomass from the 30 m ALS data across the study area.

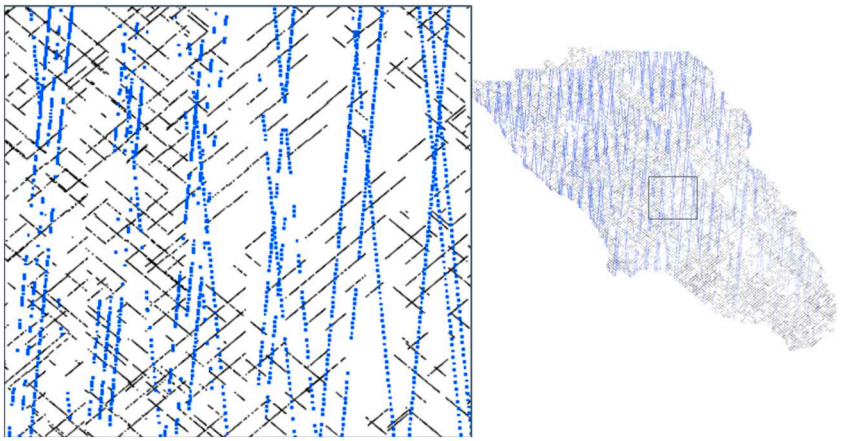

Fig. 3. UAVSAR data were acquired over the majority of the county in 2014, serving as a proxy for NISAR, while lidar mission simulations were generated representing two years of on-orbit acquisitions for both GEDI (black) and ICESat-2 (blue). (For interpretation of the references to color in this figure legend, the reader is referred to the web version of this article.)

having the same properties and expected measurement errors as GEDI. GEDI's SNR is related to beam sensitivity, i.e. the percentage of canopy cover through which we expect to be able to detect the ground 90% of the time. GEDI's power beams are expected to return a reliable ground signal beneath 99.5% canopy cover at night, and 94% canopy cover during the day, assuming 80% atmospheric transmittance with a 3db margin loss over design estimates. These increase to 97% during the day and 99.75% during the night if the 3 dB margins are maintained. Under the same conditions, the coverage beam is to produce reliable ground returns under 96% canopy cover by night and 92% canopy cover by day, increasing to 98 and 96% with preserved margins (Hancock et al., 2019).

From the simulated waveforms (Fig. 4a), the ground elevation is estimated and Relative Height (RH) metrics are extracted, which are related to biomass (Drake et al., 2002). The accuracy of these RH metrics depends on the accuracy of the ground elevation estimation for each waveform. While the GEDI mission's ground finding algorithm is still under development, for this study we used the ground finding algorithm in libClidar (Hancock et al., 2017), with denoising parameters tuned for Sonoma County. A two-year simulation of GEDI's track sampling was conducted at a global scale as part of GEDI's pre-launch mission science analysis. The sampling simulation used two-years of ISS orbits in combination with an optimized pointing algorithm to define and acquire the GEDI RGTs. These simulated orbital tracks are combined with an assumption of 50% cloud cover and filtering leaf-off data, to generate distributions of GEDI observations over the study site

(Fig. 3). GEDI metrics were extracted for biomass estimation using four noise cases representing realistic combinations of GEDI's power and coverage beams and day and night acquisitions.

2.2.3. ICESat-2 simulations

The uncertainty in the ATL08 canopy height is influenced by both the vertical sampling error as well as the solar background noise, which will impact the terrain and canopy height retrievals by the ATL08 algorithm. To simulate ICESat-2 data, the high density (~14 points m^{-2}) ALS data were sampled along five ICESat-2 ground tracks as described in Neuenschwander and Magruder (2016). The ICESat-2 frozen repeat orbit and its associated RGTs were developed as part of the mission definition and analysis. The ground tracks used in the study are those from the mission simulation and include the planned satellite off-pointing for vegetation sampling. Within each 13 m diameter simulated ICESat-2 footprint, the vertical distribution of the airborne data was taken as representative of the probability of a photon returning from a given elevation. This distribution was used to weight the random sample the "photons". The number of photons sampled for each outgoing ICESat-2 shot is based on a random selection from a Poisson distribution for the expected number of returned photons given a specific surface type. We simulate two different cases, one with an average of one photon returned per shot, and a second with an average of two photons returned per shot. Based on actual on-orbit data from ICESat-2, the average photon rate for 18 granules over Sonoma County is found to be 1.57 photons per shot with a minimum value of 0.98 photons per shot and a maximum value of 2.06 photons per shot. Thus, the data low and high photon rates utilized for the simulations in this study nicely book-end the expected performance for ICESat-2 in this region. In addition to the simulated ICESat-2 photons, canopy height metrics (RH25, RH50, RH60, RH75, RH90, RH95, and RH100) were calculated from the ALS data within each footprint for comparison. Noise was added to the sampled "photons" from the airborne lidar data to simulate various solar background conditions. The simulated dataset produces a geolocated point cloud similar to that from the ICESat-2/ATLAS measurements (ATL03) which subsequently serves as the input to the ATL08 (Land/Veg) terrain and canopy height retrieval algorithm (Neuenschwander and Pitts, 2019).

The ATL08 algorithm works by first isolating the signal photons from the noise photons in the geolocated point cloud (ATL03). Once the signal photons are identified, a ground surface and a top of canopy surface are estimated using a series of iterative filters. After the surfaces are defined, the individual photons are attributed as being reflected from the terrain or canopy based on a threshold which is a dynamic point spread function that is dependent upon the sensor uncertainty as well as geolocation and topographic uncertainty. The dynamic point spread function can vary from 50 cm to 1 m. Once the photons are attributed as either terrain, canopy, or top of canopy, they are used to calculate statistics within a 100 m step size along the ground track. For example, every 100 m, ATL08 reports statistics such as mean terrain height or standard deviation of terrain height based on the photons attributed as terrain within a 100 m step. The derivation of canopy height on the ATL08 data product is defined as the 95 percentile height of the photons attributed as canopy, where the height of each photon is calculated with respect to the terrain elevation interpolated directly beneath the photon. The RH metrics are thus calculated as the relative height of the cumulative distribution for all canopy photons, similar to how airborne lidar height percentiles are typically calculated. The output of labeled photons from the ATL08 algorithm using simulated ATLAS data over Sonoma County is shown in Fig. 4c.

2.2.4. NISAR simulations (UAVSAR)

UAVSAR is an operational fully polarimetric L-band (wavelength of 23.5 cm) synthetic aperture radar (Hensley et al., 2008) designed and operated by NASA's Jet Propulsion Laboratory to provide robust repeat pass radar interferometric measurements of deformation from both natural and anthropogenic sources. UAVSAR data were collected over Sonoma County on August 29th 2014 with a flight bearing of approximately 55°. Six flights-lines were acquired over Sonoma county. Each image is 20 km wide and approximately 155 km long, with look angles for all swaths ranging from the near to far range between 21° to 65°, respectively.

Complex topography causes increased variation in SAR imagery and limits its use over irregular terrain unless corrected for. Therefore, the radar imagery was radiometrically corrected for variations in illuminated area on the ground, as well as variations in forest reflectivity with viewing and terrain geometry using the radar look angle and range slope, as outlined by (Simard et al., 2016). The ALS digital elevation model (DEM) was merged with the SRTM DEM to cover the full extent of the UAVSAR data, and utilized to perform the radiometric correction. HH, HV and VV polarizations were processed with a native pixel spacing of 0.00005556 degrees (6.14 m at the equator). The radiometric and geometrically corrected UAVSAR imagery was re-projected to UTM and resampled to 30 m pixels to match the ALS biomass map using bilinear interpolation.

2.3. Biomass modeling

GEDI will produce global biomass products as given in GEDI L4A and L4B Algorithm Theoretical Basis Documents (Patterson et al., 2019) and these algorithms will include calibration data from a large, geographically distributed set of field sites. GEDI uses existing airborne lidar and field data and a GEDI waveform simulator to produce a global set of biomass calibration sites (see Fig. 5). The NISAR mission will produce biomass data products up to 100 Mg/ha over a select number of globally distributed sites that includes airborne and/or spaceborne L-band backscatter and ALS over a range of ecosystems. In this study, we use GEDI's L4A biomass models for simulating GEDI biomass estimates, but at the time of publication NISAR's calibration sites are not finalized, nor are the data available, so the final NISAR algorithms were not available. Instead, we developed a biomass-backscatter relationship between L-band backscatter and the Sonoma county-wide ALS biomass map. We compared height metrics from simulated GEDI and ICESat-2 in an attempt to determine whether GEDI's algorithms can be leveraged to produce ICESat-2 biomass products, and applied versions of the GEDI algorithms that only consider selection of RH metrics available in the ICESat-2 ATL08 product.

2.3.1. GEDI and ICESat-2 biomass models

For its footprint-level biomass algorithms, GEDI stratifies the globe by MODIS estimated Plant Functional Type (PFT) and region (usually continent). For Sonoma County, three GEDI models were used; one for prediction in North American Evergreen Needleleaf Trees (ENT), one for North American Evergreen Broadleaf Trees (EBT), and one for North American Woodlands, Grasslands and Shrublands (WGS) (Fig. 6). These models were also re-fit for application to ICESat-2 by only considering predictors of RH50, RH60, RH70, RH80, RH90, RH98, and their interaction terms (Fig. 7). These models were fit at the nominal GEDI resolution over GEDI-sized field plots with simulated waveforms from airborne lidar data. These are OLS models fit between square root transformed AGB and square root transformed RH metrics, with an exhaustive variable selection algorithm applied that allowed up to four predictors to be selected for each model. As with the generation of confidence intervals in the airborne reference map, the variance covariance matrices from these model fits was sampled 1000 times per model, and each iteration was applied to each simulated GEDI and ICESat-2 data point to produce confidence intervals around GEDI and ICESat-2 estimates of AGB. Please note that while Sonoma County field plots are included in GEDI's L4A model fitting, for the purposes of this paper to ensure the application was realistic to independent datasets, the Sonoma County field and lidar data were removed from GEDI's L4A database.

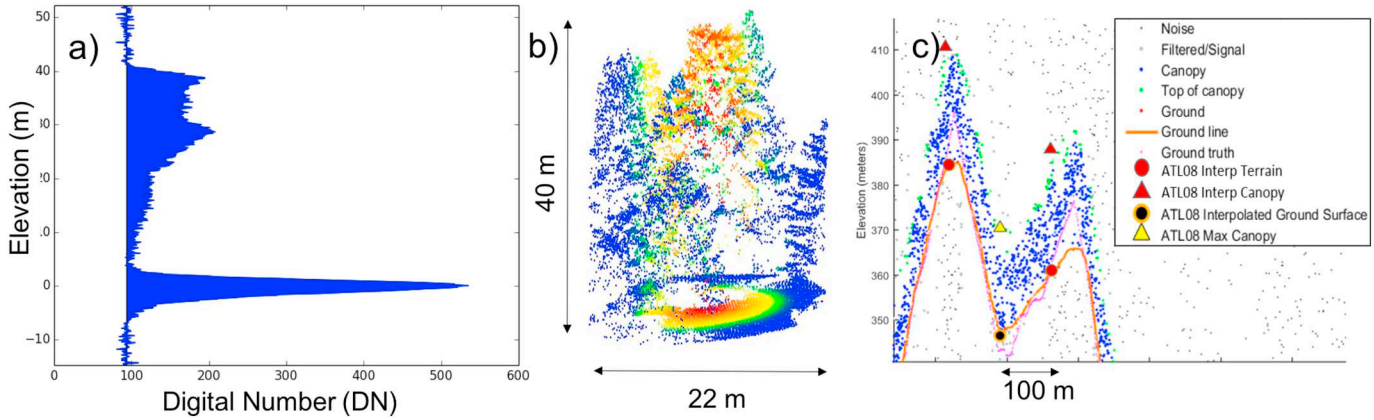

Fig. 4. Simulated GEDI waveforms (a) are vertical aggregations of point clouds (b) in GEDI sized footprints, which have been modeled to match expected pulse shape and spatial distribution of reflected energy for GEDI. ICESat-2 simulations (c) use degraded point clouds along transects with added background noise. Simulated photon returns are classified as noise, ground, or vegetation returns (c).

Fig. 5. The GEDI cal/val database for the United States was used to generate empirical models for both GEDI and ICESAT-2 from linked field plots and ALS datasets. These US-wide models were applied to the simulated GEDI & ICESAT-2 datasets in Sonoma County.

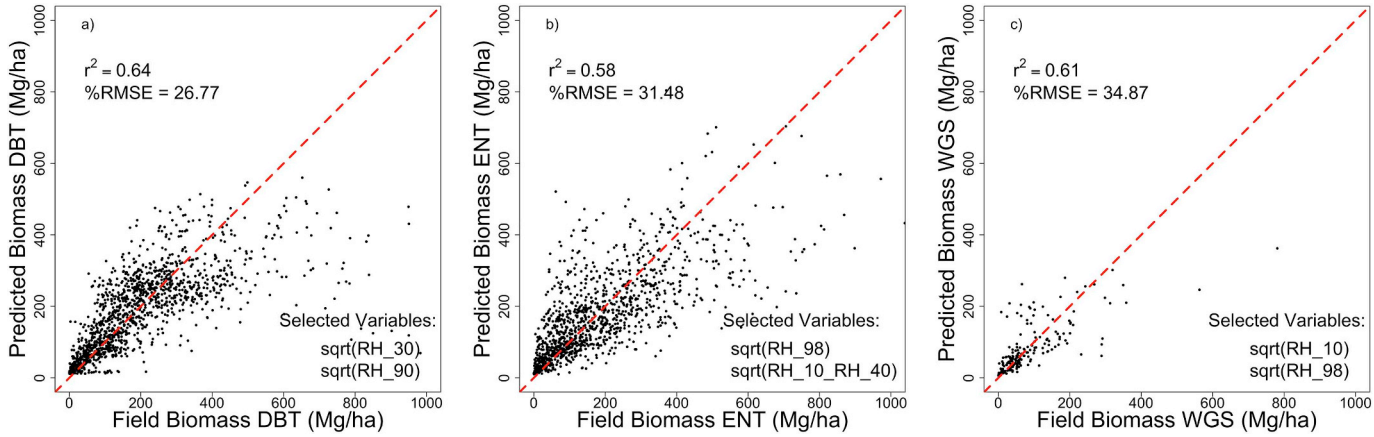

Fig. 6. The US-wide GEDI biomass model (applied to simulated GEDI) used an OLS model with exhaustive variable selection for Deciduous Broadleaf Trees (DBT), Evergreen Needleleaf Trees (ENT) and Woodland Grassland Shrub (WGS). The selected variables are displayed in the bottom right, and model accuracies are calculated by k-fold cross validation.

2.3.2. NISAR biomass model

Sonoma county presents an ambitious site for UAVSAR (and NISAR) in quantifying values of biomass which are generally in excess of the NISAR mission requirement, and within a challenging topographic environment. However, radar imaging provides a spatially continuous observation of the landscape. As such, it is possible to analyze the imagery following landscape features and patterns, and determine forest structural attributes on forest patches rather than on intrinsically square pixels or grid cells. The UAVSAR mosaic was spatially segmented into image objects using the segmentation algorithm described in Clewley et al. (2014). This utilizes k-means and iterative elimination to group similar neighboring pixels into objects of a user-defined minimum size. The UAVSAR mosaic was segmented with a minimum object size of 11 pixels, creating objects of approximately 1 ha and greater. The objects were populated with the mean HV backscatter pixel values and converted to decibel (dB). The mean ALS derived biomass, mean UAVSAR look angle and mean UAVSAR derived slope were also attributed to objects. To this effect the image objects describe the radiometric and viewing geometry characteristics of the underlying land-cover type.

SAR backscatter is known to increase with biomass up to a saturation level for a range of radar wavelengths (Luckman et al., 1998; Mitchard et al., 2009). The relationship between UAVSAR HV backscatter and ALS derived biomass was established, using image objects with a mean look angle between 33° to 47° to simulate the NISAR viewing geometry. With its 36 looks (number of pixels averaged to reduce speckle noise), UAVSAR closely simulates NISAR annual time-series with 30 ascending and 15 descending passes. Backscatter was averaged at a 5 Mg/ha biomass interval (Fig. 8b) yielding the relationship:

$$\text{HV Backscatter (db)} = -26.457 + 2.586 * \log\left[\text{Biomass (Mg/ha)}\right]$$

$$\text{Biomass (Mg/ha)} = exp\left(\frac{\text{HV Backscatter (db)} + 26.457}{2.586}\right)$$

Only objects with a mean biomass $\leq$200 Mg/ha and UAVSAR perspective slope $\leq 10^{\circ}$ were used to fit the relationship, but it was applied to all objects. We also developed backscatter models based on the full range of slopes and biomass densities, but a flat, low biomass model produced lower errors, even in sloped or higher biomass areas. This model was applied to the full area of UAVSAR coverage in Sonoma, at a minimum 1 ha scale. Residual error was generated by comparing the predicted UAVSAR biomass with the mean 30 m ALS derived biomass estimate, per image object.

2.4. Comparison to lidar reference map

For any spaceborne biomass estimate, validation using reference data is challenging given that nearly all reference data will include error. This is a challenge across the forest mapping discipline where field measurements contain uncertainties, but is particularly true of biomass which is typically estimated through the application of some allometric model e.g. (Chave et al., 2014). In this study we did not propagate error from field estimates of biomass to the reference (or spaceborne) estimates, which is consistent with comparable studies (see McRoberts et al., 2019, for an exception). However, uncertainties in field estimates of biomass are subsumed into the model fit errors, to the extent the model training data is representative of the variability driven by field plot biomass (Patterson et al., 2019). For the ALS reference map, the covariance matrix of parameter values was used to estimate model uncertainty for each pixel. Random vectors were generated from a multinomial normal distribution to create a set of 1000 realizations of the model parameters. These were then used to estimate 1000 realizations of biomass estimates. Assuming an unbiased estimator we define an interval from this resulting distribution for which the true mean response is within. We do not explicitly account for the random error of a new observation when calculating this interval, only the uncertainty in the mean of the population.

For the GEDI biomass estimates, the pixel underlying each GEDI simulated waveform centroid was used as reference. To filter footprints with spatial mismatches to the reference map (e.g. where only half a pixel is covered by GEDI) we implemented a height filter, where maximum forest height from the 30 m underlying pixel was compared to the RH99 value for simulated GEDI waveforms, calculated above ALS ground (e.g. not filtering waveforms that may have ground issues, but only those where the spatial coverage of footprints did not capture the underlying 30 m maximum height). We filtered out any waveform where this RH99 value was > 5 m different than the underlying ALS 30 m height map.

For ICESat-2, the three pixels underlying the 100 m ICESat-2 transect were extracted and averaged for reference. For NISAR, all of the reference pixels were averaged at a 1 ha resolution for comparison to L-band backscatter estimates, and there was no spatial mismatch because of the wall-to-wall sampling of the SAR data.

The statistical comparison of simulated spaceborne estimates to reference estimates was conducted by computing confidence intervals around both sets of predictions. In reference pixels with high uncertainties, we are unable to 'validate' the spaceborne estimates; indeed, if the confidence intervals between the ALS and simulated spaceborne estimates overlap, there is no discernable error in the spaceborne estimates insofar as the reference map can detect. This does not, however, mean the spaceborne estimate is without error. Conversely, if there is no overlap between these 90th percentile confidence intervals, (i.e. the minimum from the reference map is still greater than the maximum from the spaceborne estimate) we can determine that the uncertainties in the spaceborne estimate are underestimated. In sum, we can only validate that spaceborne estimates are correct to the accuracy level of the reference map, but we can determine when spaceborne estimates are definitively incorrect. To achieve this, we calculated the percentage of estimates for each mission that had per pixel overlapping confidence intervals with the corresponding reference map, and attempted to explain observe errors as a function of environment. This is reported in addition to more traditional differences in means between reference and spaceborne estimates.

In addition to biomass estimates, the county-wide airborne lidar dataset was used to generate 30 m resolution maps of terrain slope, forest canopy height and percent canopy cover. These maps were used to assess the impact of these variables on biomass estimation accuracy. The slope, height, and cover maps were extracted to match the simulated spaceborne resolutions the same way the biomass map was used for comparison. For the comparison of NISAR estimates to slope we used SAR observed slope rather than absolute slope, as the SAR signals are affected by topography depending on the look angle of the sensor, with topography either facing away from the sensor (typically decreasing backscatter) or toward the sensor (typically increasing backscatter).

2.5. Comparison of ICESat-2 and GEDI height metrics

To explore the utility of GEDI's biomass algorithms to ICESat-2 data, we also simulated GEDI footprints at the midpoint of ICESat-2100-m transects across Sonoma. Considering differences between GEDI and ICESat-2 instruments and datasets (wavelength, spatial resolution, calculation of RH metrics, etc.) we calculated the biases between RH95, RH75, RH50 and RH25 between simulations of GEDI's power beam collected in nighttime (low noise) conditions, and the two sets of ICESat-2 simulations. We also compared the ALS heights to GEDI and ICESat-2 estimated heights following the same approach for extracting reference values as for the biomass evaluation, and compared residuals as a function of environment.

3. Results

The biomass residuals from the three simulated missions (Fig. 9), as calculated by comparison to the ALS reference map at their nominal resolutions, vary as a function of maximum canopy height, percent canopy cover, and terrain slope (Fig. 10). Note that Figs. 9 and 10 include all estimates, regardless of whether there were overlapping confidence intervals. The relative accuracies of each of these datasets is presented in Table 2 with respect to the ALS reference estimates at each resolution, where the % confidence interval overlap is the percentage of estimates where the 90th percentile confidence intervals from the reference and spaceborne estimates overlap, RMSE is the square root of the mean squared residuals, mean bias is calculated as the mean residuals (with respect to the ALS map), %RMSE and % bias divides these statistics by the mean reference biomass at each resolution, and slope is the slope of a linear model fit between spaceborne estimates and the reference map. The distance between the extremes of the reference confidence interval and simulated spaceborne confidence intervals are also dependent on environmental gradients (SI Fig. 2). As expected, GEDI errors also increase as a function of biomass, with higher

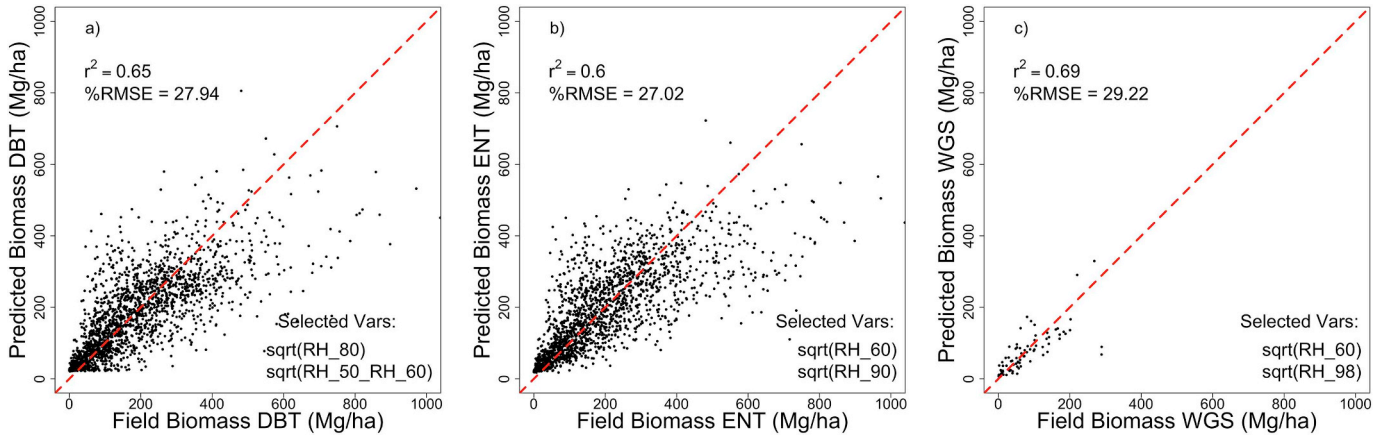

Fig. 7. The US-wide GEDI biomass models allowing only selection of variables available in the ICESat-2 ATL08 algorithm for Deciduous Broadleaf Trees (DBT), Evergreen Needleleaf Trees (ENT) and Woodland Grassland Shrub (WGS) These models were applied to simulated ICESat-2 data across the study area.

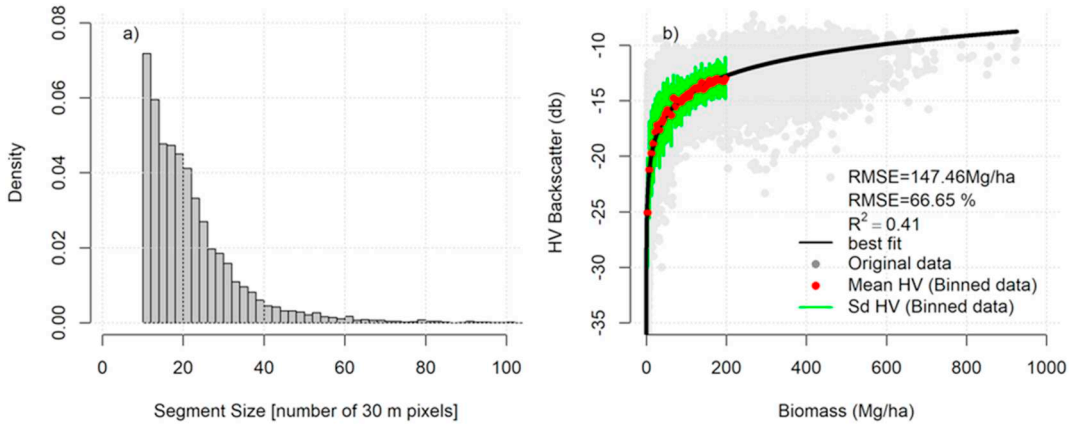

Fig. 8. The study area was segmented based on UAVSAR backscatter. A) shows a histogram of the object sizes (number of 30 m pixels). The average HV backscatter per biomass bin was used to generate a backscatter to biomass curve (b). The black solid line is the best fit, and the vertical green lines represent the standard deviation of HV Backscatter in each biomass bin. The gray dots are the average of HV backscatter and biomass data per object. (For interpretation of the references to colour in this figure legend, the reader is referred to the web version of this article.)

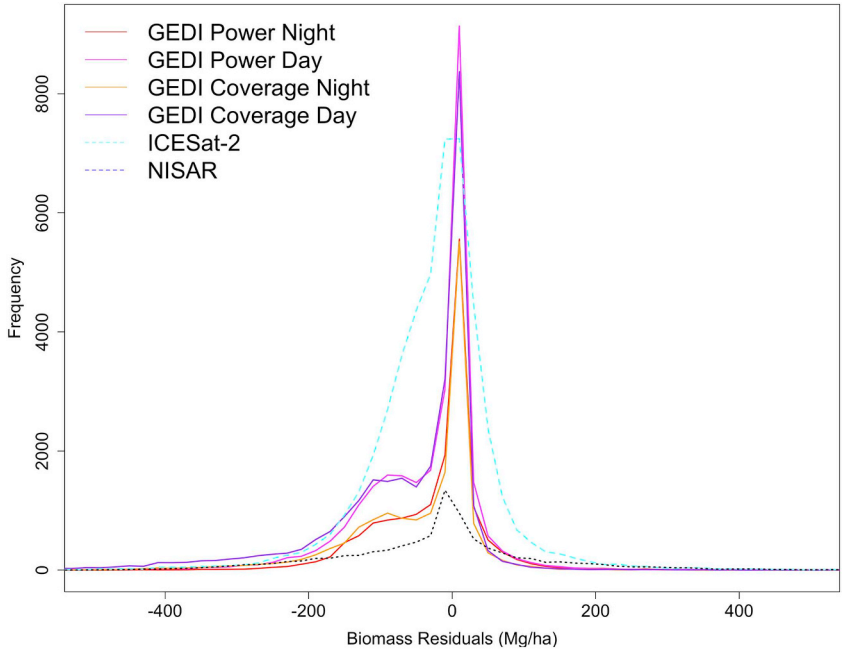

Fig. 9. Histograms showing the relative distribution of residuals (simulated mission estimates in comparison to the reference biomass map) from each mission. Note that here low-photon rate ICESat-2 simulations were used.

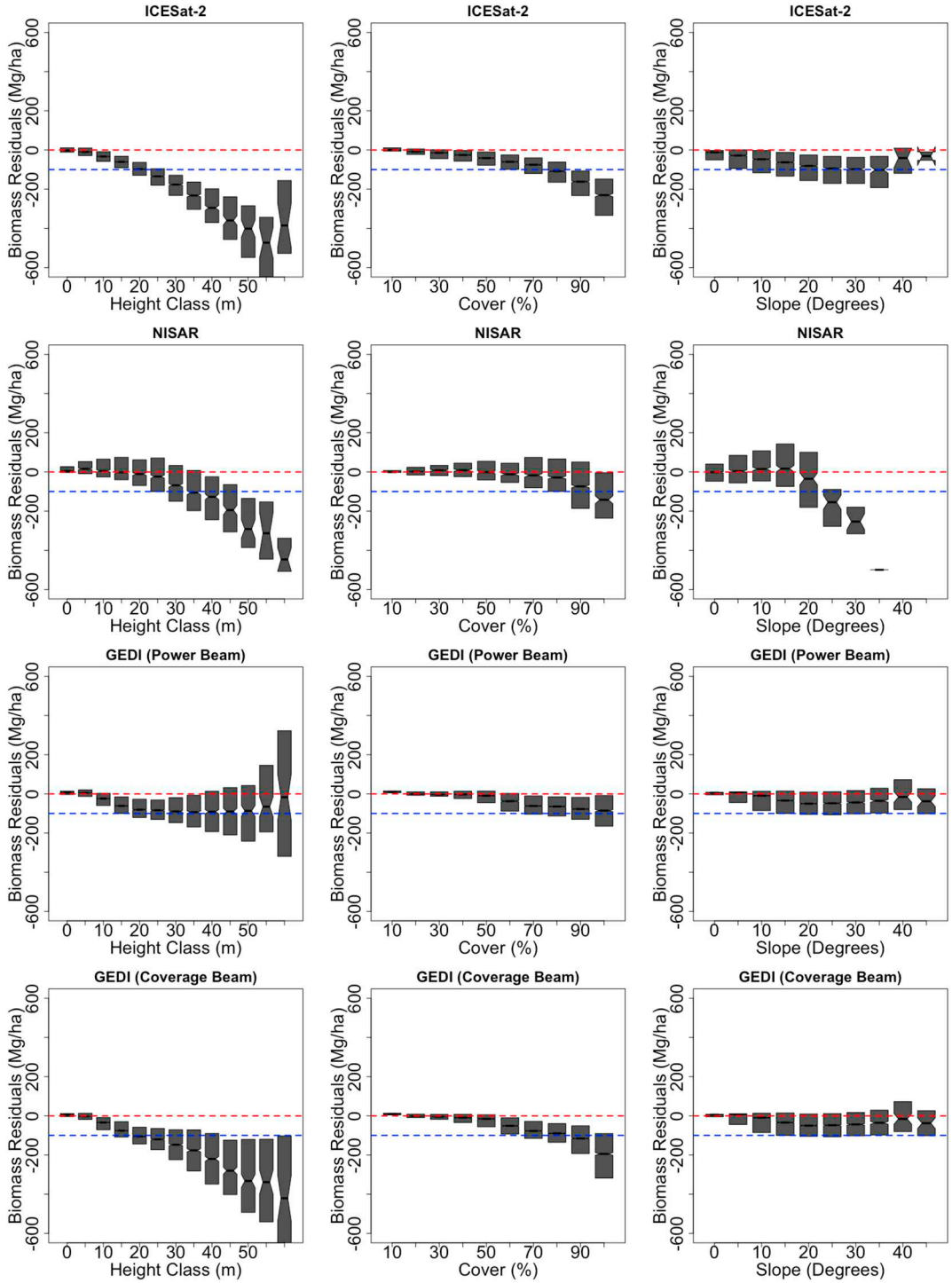

Fig. 10. ICESat-2 residuals (a–c), NISAR residuals (d–f), GEDI power beam residuals (g–i), and GEDI coverage beam residuals (j–l) plotted as a function of canopy height, % canopy cover, and slope. Each mission's residuals are presented with respect to ALS estimated biomass at their native resolution, i.e. footprint-level (25 m) for GEDI, 100 m transects for ICESat-2, and 1 ha for NISAR (UAVSAR). The blue dotted lines are plotted for comparison at negative 100 Mg/ha of biomass. The blue dotted line represents −100 Mg/ha. (For interpretation of the references to colour in this figure legend, the reader is referred to the web version of this article.)

sensitivity of errors to biomass seen in daytime and coverage beam simulations (Fig. 11). ICESat-2 errors are also sensitive to biomass, particularly for the low photon rate simulations (Fig. 12). We also compared the realistic ICESat-2 rate height metrics to simulated GEDI height metrics at the same locations to explore limitations to the transferability of GEDI's models to ICESat-2, and found that particularly for the low photon rate biases between the two sets of height metrics likely limit the accuracy of ICESat-2 for biomass estimation using this approach (Fig. 13). However, we also found that ICESat-2 and GEDI coverage beams underestimated height particularly in tall forests (SI Fig. 5), suggesting biomass estimation for weaker beams is primarily limited by height estimation regardless of the biomass model selection.

3.1. GEDI biomass residuals

GEDI's power beam biomass estimates yield the lowest deviations

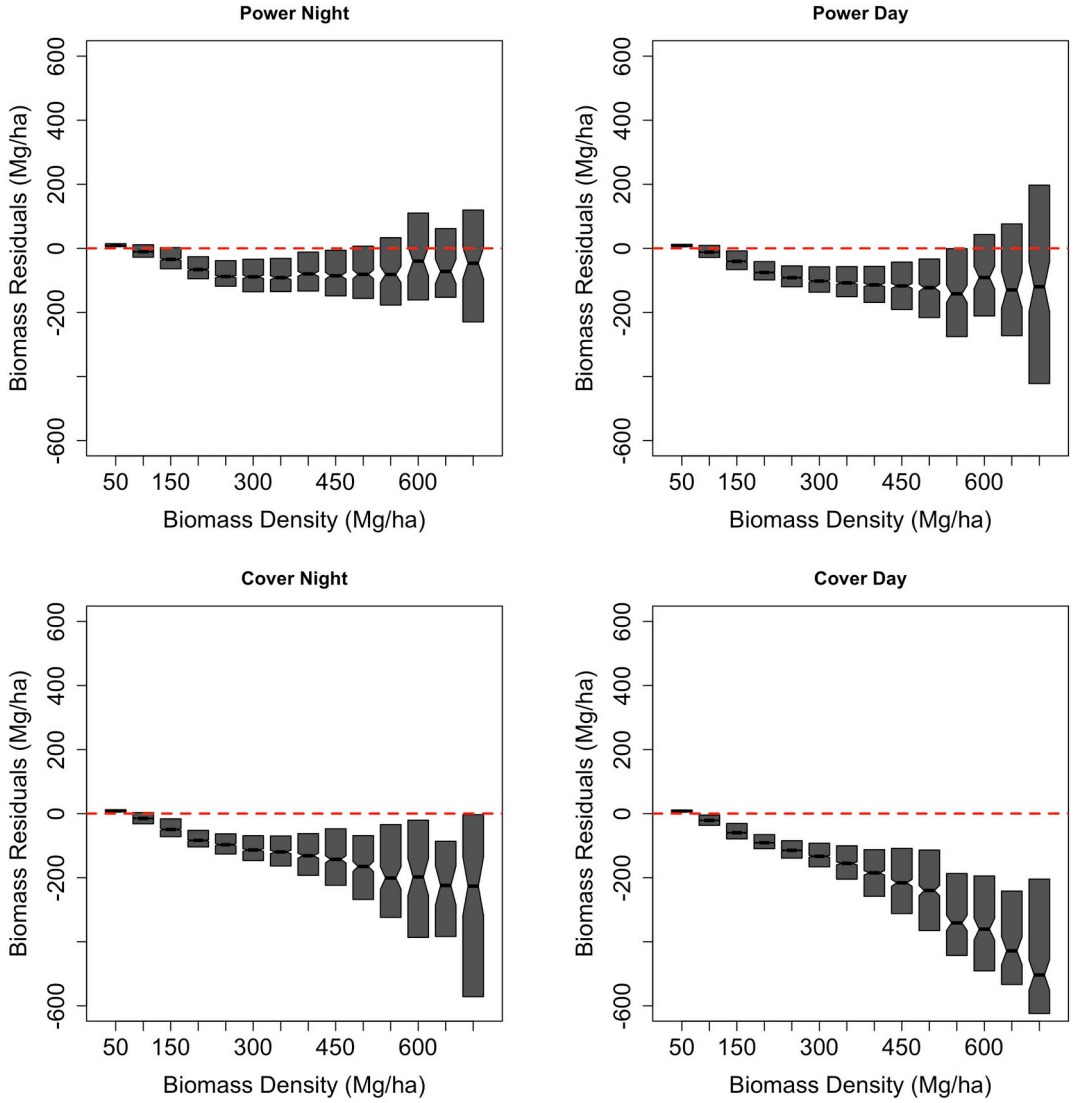

Fig. 11. Simulated GEDI biomass residuals as a function of reference biomass bin, plotted for each of our four GEDI simulation scenarios.

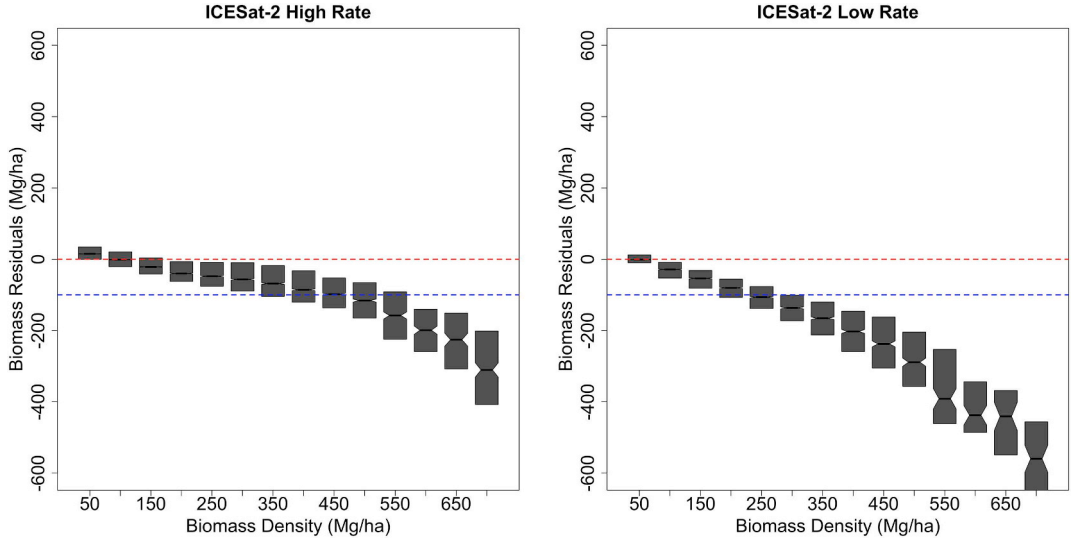

Fig. 12. Higher signal photon rates for ICESat-2 (a) decrease biomass estimations by ~50% in each reference biomass bin, but even high photon rates still yield underestimates of biomass beyond ~500 Mg/ha. The blue dotted line represents −100 Mg/ha. (For interpretation of the references to colour in this figure legend, the reader is referred to the web version of this article.)

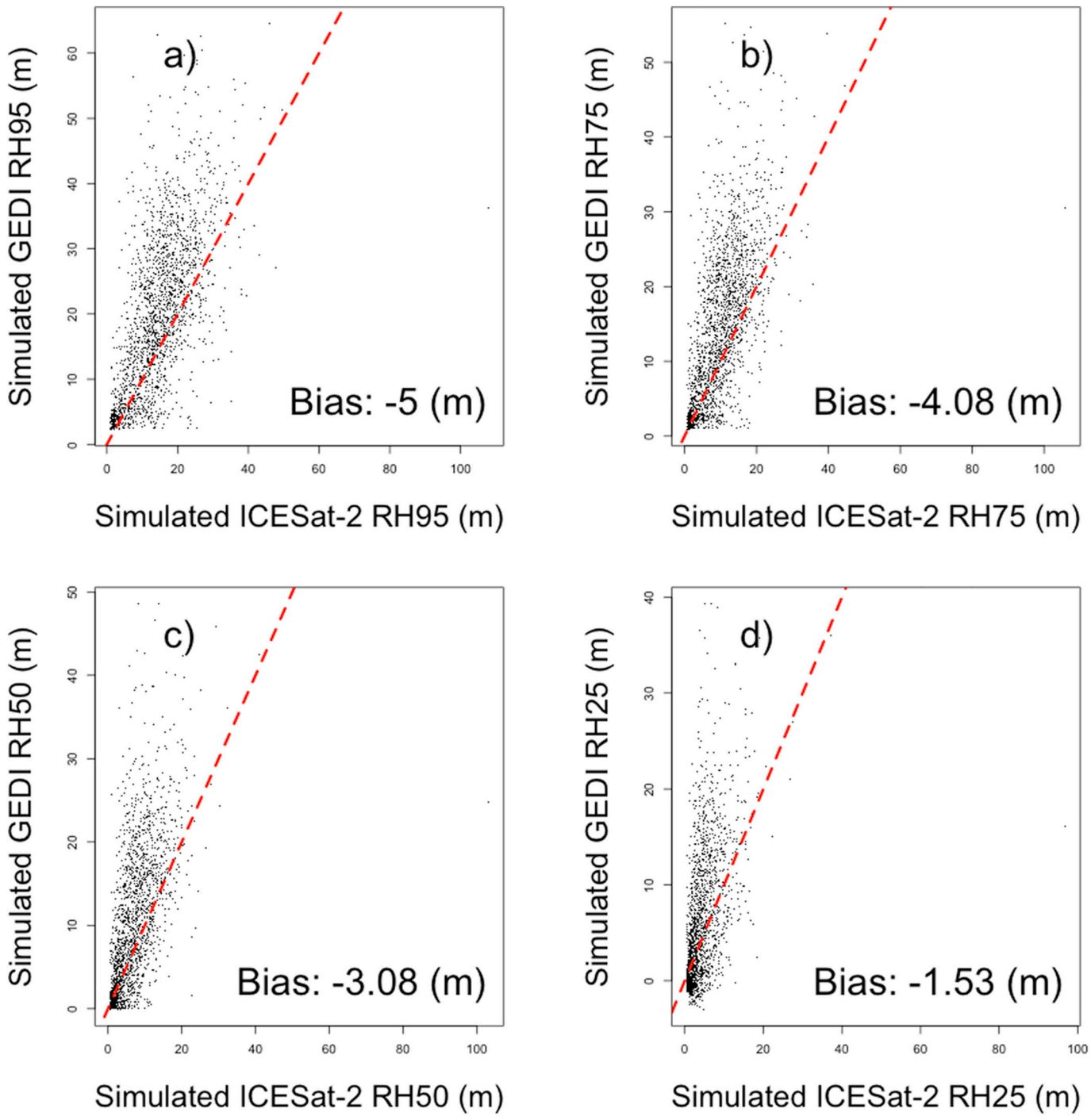

Fig. 13. A comparison of simulated GEDI RH metrics to the lower signal photon return rate ICESat-2 estimations shows that ICESat-2 underestimates height, particularly in the higher height metrics (e.g. RH95). These underestimates of height partially explain underestimates of biomass from simulated ICESat-2.

from the reference map both on average and in high biomass, tall, dense forests compared to any other simulated spaceborne estimate in this study. The power beam also has the highest percentage of overlapping confidence intervals, indicating that not only are the mean values closest to the reference values, but the uncertainties estimated for the GEDI power beam data were accurately reported almost 60% of the time. On average, the GEDI power beam data still slightly underestimates biomass in Sonoma County, but these underestimates are modest across ranges of topography and forest structure. A comparison between the GEDI power and coverage beams, Figs. 10, 12, and SI Fig. 5, suggests that the majority of errors in simulated GEDI biomass estimates come from errors in the height metric estimates in the coverage beam data rather than errors in the GEDI biomass model. Additionally, topographic slope does not appear to drive errors in either the power or coverage beam data (Fig. 10, SI Fig. 5).

3.2. NISAR biomass residuals

While NISAR residuals are generally unbiased in areas of low canopy cover and slope, over slopes steeper than ~20° or forests taller than ~25 m NISAR underestimates biomass by > 100 Mg/ha (Fig. 10), with increasing underestimation in taller forests or over steeper slopes. These errors are likely due to saturation issues in the backscatter signal, as expected for L-band SAR, but the good performance in shorter, lower

Table 2
Assessment of each simulated mission dataset calculated with respect to the reference airborne lidar biomass map at 30 m (GEDI), 3 × 30 m (ICESat-2), and 1 ha (NISAR).

Mission	Scenario	%Confidence overlap	RMSE (Mg/ha)	%RMSE (Mg/ha)	Mean bias (Mg/ha)	%Bias mean	Slope
GEDI	Power night	58.4	80.2	57.1	−26.3	−18.7	0.81
GEDI	Power day	56	93.1	64.5	−38	−26.3	0.72
GEDI	Coverage night	54.2	105.5	71.7	−47.8	−32.5	0.64
GEDI	Coverage day	50.8	128.8	87.6	−64.2	−43.7	0.49
NISAR	All bio	34.6	151.55	74.9	−7.47	−0.03	0.73
NISAR	Low bio	46.5	101.7	288	−37.4	−0.5	0.17
ICESat-2	High photon return	47.6	106.4	59	−23.34	−13%	0.69
ICESat-2	Low photon return	34.9	137.8	89.1	−72.11	−47%	0.4

canopy cover forests shows promise for the utility of fusion algorithms to extend lidar samples toward wall-to-wall mapping.

3.3. ICESat-2 biomass residuals

For ICESat-2, we focus our analysis on the lower signal photon rate simulations because they match the photon rates of the limited on-orbit ICESat-2 data that have been collected over Sonoma County at the time of writing. As seen in Fig. 10, ICESat-2 underestimates biomass on average, and this underestimation increases with canopy height, canopy cover, and to a small degree with slope. The comparison between simulated GEDI and ICESat-2 height metrics (Fig. 13) confirms that at least with respect to GEDI simulations, ICESat-2 underestimates height, and these underestimations are more pronounced in the higher height metrics. Further, SI Fig. 5 shows that the same trends in height error with respect to ALS height match the trends found in biomass estimation errors. However, a comparison of ICESat-2 simulations from the higher signal photon return rate (SI Fig. 3, SI Fig. 4) shows that the signal rate drives much of this error, so in areas where ICESat-2 has little atmospheric attenuation ICESat-2 will likely perform well for forest structure.

4. Discussion

4.1. Utility of airborne lidar reference maps for validation

Our multi-mission inter-comparison depended entirely on the availability of a high-quality regional reference map that is trained with field data across the range of conditions found in Sonoma County. The spatial configuration of both NISAR and ICESat-2 mean that field plots are typically not readily available for direct comparison to spaceborne missions. Even for GEDI, when small field plots are available, geolocation errors in the field data and/or GEDI data will add errors to the calibration and validation process (Réjou-Méchain et al., 2019). Airborne lidar is an ideal tool for scaling between field plots and satellite datasets, as has been widely documented. Additional advantages highlighted in this study are the ability to explain errors in satellite datasets as a function of structural gradients, both of vegetation and the underlying terrain. Further, the ability to aggregate high resolution lidar biomass maps to the appropriate spatial resolution of a given satellite product allows for the comparison of multi-mission datasets over the same set of environmental conditions, enabling a more thorough evaluation of the strengths and limitations of each dataset toward informed data fusion.

While ALS biomass maps allow for simple scaling to multiple mission resolutions, the interpretation of the results in this paper should be caveated by the different spatial scales analyzed. It is well accepted that biomass model fitting errors reduce with increasing plot size or resolution (Hall et al., 2011; Labriere et al., 2018; Zolkos et al., 2013), partially because of reductions in edge effects, but largely because of the reduced variance in the biomass values with increases in spatial scale. Therefore, the results in this study cannot be directly quantitatively compared because the estimation and validation were at three different resolutions. Additionally, our airborne biomass estimates only accounted for uncertainty in the mean of the population and ignored the uncertainty in individual observations. There remain a lack of studies that comprehensively account for sources of measurement and model error in spaceborne estimates and ALS reference maps for such comparisons. A review of existing methods and recommendations for best practice are currently the subject of the forthcoming CEOS LPV Biomass validation protocol (Duncanson et al., 2019).

This research involved the utility of airborne lidar biomass maps for validation, and focused on understanding expected errors in biomass products from upcoming GEDI, ICESat-2 and NISAR datasets, and there are several important caveats in the interpretation of this work. First, we present a simplified version of simulated estimates from three sensors and this work is not fully representative of finalized mission algorithms. Trends between errors and environmental gradients will differ for other areas, e.g. in different forest types such as in the tropics. Additionally, although we expect mission algorithms to be generally similar to those adopted here, the final GEDI models and ground finding algorithms will likely vary in specificity, variable selection, parameterization, and ultimately accuracy. The NISAR models, similarly, will differ from those shown here, as they will be generalized across biomes rather than locally fit, focused on relatively simpler, lower biomass systems than those in this study, and be based on temporal composites of L-band backscatter rather than the single date UAVSAR data used in this study.

4.2. Interpretation of simulated mission biomass estimation accuracies

In this paper we focus on developing and implementing algorithms as similar as currently possible to those used by mission teams to produce biomass estimates at the aforementioned resolutions, although we expect a large number of researchers will develop their own biomass algorithms for particular applications. Thus, these algorithms can be thought of as reasonable approximations for expected estimates of biomass from the upcoming missions, but by no means represent the only approach one may take to estimate biomass with GEDI, ICESat-2, or NISAR. Similarly, neither of the simulated lidar mission datasets are used here to produce a gridded product akin to what the mission teams will release, but can be thought of as similar to what GEDI's footprint level biomass product will produce, and similar to a possible transect-level product from ICESat-2.

Overall, these upcoming missions performed as one might expect in such a challenging, high biomass system. Sonoma County presents a wide range of biomass densities, with the mean biomass far above the expected saturation limit for optical and even L-band SAR systems. As such, we anticipated saturation in the NISAR simulations, and high RMSE values for the lidar systems. In addition to high biomass densities, the steep slopes found in much of Sonoma increase errors in height retrievals and biomass estimates, which was also expected. Considering the application of generalized biomass models to these spaceborne lidar simulations, we find these results are generally in line

with expected mission performance, and feel they highlight environmental domains that will remain challenging for this next generation of datasets. Indeed, we feel this study highlights areas where further research and algorithm refinement would be particularly beneficial.

We found that for the lidar missions, height retrieval accuracy was the primary driver of biomass error estimation, with errors more highly related to forest structure than to terrain slope. As expected, the highest accuracies were from GEDI's power beam, while accuracies for ICESat-2 depended heavily on the signal photon rate, and NISAR accuracies will depend on the availability of high-quality biomass training data, and be limited to lower biomass forests over relatively flat areas. Nonetheless, we find all three sets of mission simulations promising for biomass. From a GEDI perspective, the simulated estimates had the highest accuracies as expected and certainly performance is well within mission requirements. Considering that Sonoma County hosts some of the highest biomass densities in the United States, many of which are growing over steep slopes, this is indeed an encouraging result. As expected, errors in GEDI heights, and therefore biomass estimates increase for the coverage beams, particularly when acquired during the daytime.

Also encouraging is the relative success of applying GEDI's footprint level biomass algorithms to ICESat-2. As ICESat-2 does not have a mission requirement for forest structure or biomass, this ICESat-2 work was largely exploratory, and Sonoma County presents an interesting test bed for ICESat-2. It is important to note that while we adapted GEDI's algorithms to only consider RH metrics available in the ICESat-2 vegetation product for model development, these models were fit at the GEDI resolution, not the ICESat-2 resolution, and for a robust development of ICESat-2 models we would recommend fitting models at the ICESat-2 resolution. Unfortunately, considering that few field plots exist that are large enough, and stem-mapped to enable extraction of 100 m by 13 m plots, we expect ICESat-2 model development will either involve adaption of GEDI's models (as in this study), or leverage high resolution, locally calibrated ALS biomass maps that enable the extraction of any reference size and shape. As expected, ICESat-2 underestimates heights, particularly in dense, tall forests, and therefore may not be appropriate for biomass mapping under all conditions. As with GEDI's coverage beam acquired during the day, it may be desirable to filter ICESat-2 data in dense forests. Based on our analysis, we would recommend caution when using low photon return rate ICESat-2 for biomass estimation in areas of > ~60% canopy cover. However, as seen in Fig. 3, the spatial pattern of ICESat-2 is complementary to GEDI, and thus even a subset of ICESat-2 data should bolster fused forest structure mapping activities, particularly in areas with relatively open canopies (e.g. woodlands, plantations, alpine and boreal forests). In this study, high photon return rate ICESat-2 simulations could adequately detect the ground for biomass estimation, which shows promise for the utility of ICESat-2 even in areas of high biomass. However, other biomass rich areas such as the tropics may present greater difficulties. Ecosystem requirements for biomass as explained in (Hall et al., 2011) have specified that accuracies of about 1 m in height will be required for many science applications. Thus, further research should focus on how to reduce these biases, especially with an eye toward the eventual creation of blended GEDI/ICESat-2 height products, and any biomass products generated from these.

While the sampling lidar missions show tremendous promise toward accurate global forest structure datasets, many applications (e.g. for land managers) require wall-to-wall mapping. Our NISAR results are also encouraging, in that L-band SAR data were able to estimated biomass even in relatively dense canopies (up to ~70% canopy cover), which corresponds roughly to 100 Mg/ha in Sonoma, approximately the expected saturation limit of L-band backscatter. It should be reemphasized that for our NISAR simulations, the biomass estimates in this study were trained with the reference biomass map, and therefore biases were not realistically assessed, we anticipate that NISAR biomass estimates will likely be trained with GEDI (and potentially ICESat-2) in the future. Even using the simplistic methods adopted here would enable the extension of the lidar samples to wall-to-wall maps, and we fully anticipate more sophisticated approaches will be developed once NISAR data are available to the scientific community.

When looked at as an ensemble of observations, the combination of all three mission datasets potentially provides an interesting range of capabilities that spans high biomass, high cover and repeated and global coverage. When used together, there is the potential to generate biomass products that are more accurate and/or of higher resolution than what any one mission could produce by itself. But as noted above, an informative first step is a comparison of biomass estimation errors from all three missions separately, as conducted in this paper. The methods presented here allow interpretation of biomass estimation errors from these three simulated mission datasets over the same range of environmental conditions, allowing a comparison of the general strengths and weaknesses of each.

5. Conclusions

We are entering an exciting era for active remote sensing of forests, with a wealth of upcoming datasets sensitive to forest structure. We anticipate many new forest biomass products will be generated through various combinations of these next generation datasets, and while this is desirable, the consistent comparison of forthcoming products is critical to the continued improvement of algorithms and adoption of products for a wide range of applications. This paper focuses on comparing simulated biomass estimates from three new and upcoming missions, GEDI, ICESat-2 and NISAR, that will each collect a different type of data useful to varying degrees for biomass mapping. Although ICESat-2 does not have a mission science requirement of biomass products, and NISAR only has a requirement to be able to estimate biomass < 100 Mg/ha, we have explored the impact of topography and forest structure on estimating biomass from each of these missions, focusing on a structurally complex temperate forested ecosystem. Our results have shown that each mission, by itself, will perform differently under varying environmental conditions, which was expected. Only one of the missions, GEDI, was specifically designed to retrieve vegetation structure and biomass under a large range of environmental conditions sufficient to meet biomass mapping requirements as specified by the ecosystem community. However, both NISAR and ICESat-2 will provide exceptionally valuable observations for biomass mapping, providing global observations, and in the case of NISAR all-weather capability and very high-temporal resolution. One needs only to look at the examples of ALOS PALSAR and ICESat (GLAS) to understand the impact that missions, whose main foci are not ecosystem structure, may have on biomass mapping.

Looking forward, it is reasonable to expect users to want to use the data from all three missions for various applications. Whether they should use all the data is a different question and will rest in large part on how well the errors of using any particular data set can be characterized. Until all three missions are in orbit and collecting data, we will not know for certain what the true capability of each system is, nor how this may change with time. In this sense, our work provides a preview of what might influence the accuracy of each data product, and what an end-user might expect when evaluating whether to embark along a path of multi-sensor mapping using GEDI, NISAR and ICESat-2.

Supplementary data to this article can be found online at https://doi.org/10.1016/j.rse.2020.111779.

CRediT authorship contribution statement

L. Duncanson: Conceptualization, Data curation, Formal analysis, Investigation, Validation, Visualization, Writing - original draft.**A. Neuenschwander:**Investigation, Formal analysis, Visualization, Writing - review & editing.**S. Hancock:**Formal analysis, Writing - original draft.**N. Thomas:**Formal analysis, Writing -

original draft.**L. Fatoyinbo:**Investigation, Writing - review & editing.**M. Simard:**Investigation, Supervision, Writing - review & editing.**C. Silva:**Formal analysis, Visualization, Writing - original draft.**J. Armston:**Conceptualization, Writing - review & editing.**S. Luthcke:**Data curation, Formal analysis.**M. Hofton:**Investigation.**J. Kellner:**Formal analysis, Writing - original draft.**R. Dubayah:**Writing - original draft, Methodology.

Declaration of competing interest

The authors declare that they have no known competing financial interests or personal relationships that could have appeared to influence the work reported in this paper.

Acknowledgements

This work was primarily funded through NASA's Terrestrial Ecology Program and NASAs Carbon Monitoring System (CMS, grant NNH15ZDA001N-CMS), and the authors gratefully acknowledge additional support for coauthors Hancock, Armston, Kellner and Dubayah by a NASA contract to the University of Maryland for the Global Ecosystem Dynamics Investigation, and additional support for Amy Neuenschwander through ICESat-2 (NASA HQ NNX17AG55G). This work involved significant contributions from many other individuals on mission teams, and we would like to particularly thank Paul Patterson and Sean Healey for helpful input in the development of the lidar biomass models applied here. We also gratefully acknowledge Mike Falkowski, Andy Hudak, Patrick Fakety, Warren Cohen, Hans Anderson, and Luigi Boscetti for provision of the US field and airborne lidar used to generate the lidar algorithms in this study (published in a separate paper), and Suzanne Marselis and David Minor for data processing and database management. Additional thanks to Kaitlin Harbeck for helping produce the simulated ICESat-2 data, and Katherine Pitts for running the ATL08 algorithm on the simulated ICESat-2 data.

References

Baccini, A., Goetz, S.J., Walker, W.S., Laporte, N.T., Sun, M., Sulla-Menashe, D., Hackler, J., Beck, P.S.A., Dubayah, R., Friedl, M.A., Samanta, S., Houghton, R.A., 2012. Estimated carbon dioxide emissions from tropical deforestation improved by carbon-density maps. Nat. Clim. Chang. 2, 182–185. https://doi.org/10.1038/nclimate1354.

Blair, J.B., Hofton, M.A., 1999. Modeling laser altimeter return waveforms over complex vegetation using high-resolution elevation data. Geophys. Res. Lett. 26, 2509–2512. https://doi.org/10.1029/1999GL010484.

Chave, J., Réjou-Méchain, M., Búrquez, A., Chidumayo, E., Colgan, M.S., Delitti, W.B.C., Duque, A., Eid, T., Fearnside, P.M., Goodman, R.C., Henry, M., Martínez-Yrízar, A., Mugasha, W.A., Muller-Landau, H.C., Mencuccini, M., Nelson, B.W., Ngomanda, A., Nogueira, E.M., Ortiz-Malavassi, E., Pélissier, R., Ploton, P., Ryan, C.M., Saldarriaga, J.G., Vieilledent, G., 2014. Improved allometric models to estimate the aboveground biomass of tropical trees. Glob. Change Biol. 20, 3177–3190. https://doi.org/10.1111/gcb.12629.

Chen, Q., 2010. Retrieving vegetation height of forests and woodlands over mountainous areas in the Pacific Coast region using satellite laser altimetry. Remote Sens. Environ. 114, 1610–1627. https://doi.org/10.1016/j.rse.2010.02.016.

Clark, D.B., Kellner, J.R., 2012. Tropical forest biomass estimation and the fallacy of misplaced concreteness. J. Veg. Sci. 23, 1191–1196. https://doi.org/10.1111/j.1654-1103.2012.01471.x.

Clewley, D., Bunting, P., Shepherd, J., Gillingham, S., Flood, N., Dymond, J., Lucas, R., Armston, J., Moghaddam, M., 2014. A python-based open source system for geographic object-based image analysis (GEOBIA) utilizing raster attribute tables. Remote Sens. 6, 6111–6135. https://doi.org/10.3390/rs6076111.

Davidson, F.M., Sun, X., 1988. Gaussian approximation versus nearly exact performance analysis of optical communication systems with PPM signaling and APD receivers. IEEE Trans. Commun. 36, 1185–1192. https://doi.org/10.1109/26.8924.

Drake, J.B., Dubayah, R.O., Knox, R.G., Clark, D.B., Blair, J.B., 2002. Sensitivity of large-footprint lidar to canopy structure and biomass in a neotropical rainforest. Remote Sens. Environ. 81, 378–392.

Dubayah, R, 2020. Science of Remote Sensing. https://doi.org/10.1016/j.srs.2020.100002.

Dubayah, R., Swatantran, A., Huang, W., Duncanson, L., Tang, H., Johnson, K., Hurtt, G.C., 2013. CMS: LiDAR-derived Biomass, Canopy Height and Cover, Sonoma County, California, 2013.

Dubayah, R., Blair, J.B., Goetz, S., Fatoyinbo, L., Hansen, M., Healey, S., ... Armston, J., 2020. The Global Ecosystem Dynamics Investigation: High-resolution laser ranging of the Earth's forests and topography. Mapp. Sci. Remote. Sens. 1 (100002).

Duncanson, L., Huang, W., Johnson, K., Swatantran, A., McRoberts, R.E., Dubayah, R., 2017. Implications of allometric model selection for county-level biomass mapping. Carbon Balance Manag 12. https://doi.org/10.1186/s13021-017-0086-9.

Duncanson, L., Armston, J., Disney, M., Avitabile, V., Barbier, N., Calders, K., Carter, S., Chave, J., Herold, M., Crowther, T.W., Falkowski, M., Kellner, J.R., Labrière, N., Lucas, R., MacBean, N., McRoberts, R.E., Meyer, V., Næsset, E., Nickeson, J.E., Paul, K.I., Phillips, O.L., Réjou-Méchain, M., Román, M., Roxburgh, S., Saatchi, S., Schepaschenko, D., Scipal, K., Siqueira, P.R., Whitehurst, A., Williams, M., 2019. The importance of consistent global Forest aboveground biomass product validation. Surv. Geophys. 40, 979–999. https://doi.org/10.1007/s10712-019-09538-8.

Duncanson, L.I., Niemann, K.O., Wulder, M.A., 2010. Estimating forest canopy height and terrain relief from GLAS waveform metrics. Remote Sens. Environ. 114, 138–154. https://doi.org/10.1016/j.rse.2009.08.018.

Hall, F.G., Bergen, K., Blair, J.B., Dubayah, R., Houghton, R., Hurtt, G., Kellndorfer, J., Lefsky, M., Ranson, J., Saatchi, S., Shugart, H.H., Wickland, D., 2011. Characterizing 3D vegetation structure from space: Mission requirements. Remote Sens. Environ. 115, 2753–2775. https://doi.org/10.1016/j.rse.2011.01.024.

Hancock, S., Disney, M., Muller, J.-P., Lewis, P., Foster, M., 2011. A threshold insensitive method for locating the forest canopy top with waveform lidar. Remote Sens. Environ. 115, 3286–3297.

Hancock, S., Anderson, K., Disney, M., Gaston, K.J., 2017. Measurement of fine-spatial-resolution 3D vegetation structure with airborne waveform lidar: Calibration and validation with voxelised terrestrial lidar. Remote Sens. Environ. 188, 37–50.

Hancock, S., Armston, J., Hofton, M., Sun, X., Tang, H., Duncanson, L.I., Kellner, J.R., Dubayah, R., 2019. The GEDI simulator: a large-footprint waveform lidar simulator for calibration and validation of spaceborne missions. Earth Space Sci. https://doi.org/10.1029/2018EA000506.

Hensley, S., Wheeler, K., Sadowy, G., Jones, C., Shaffer, S., Zebker, H., ... Vines, K., 2008. The UAVSAR instrument: Description and first results. In 2008 IEEE Radar Conference. IEEE, pp. 1–6.

Hilbert, C., Schmullius, C., 2012. Influence of surface topography on ICESat/GLAS Forest height estimation and waveform shape. Remote Sens. 4, 2210–2235. https://doi.org/10.3390/rs4082210.

Homer, C., Dewitz, J., Yang, L., Jin, S., Danielson, P., Xian, G., Coulston, J., Herold, N., Wickham, J., Megown, K., 2015. Completion of the 2011 National Land Cover Database for the conterminous United States–representing a decade of land cover change information. Photogramm. Eng. Remote. Sens. 81, 345–354.

Houghton, R.A., House, J.I., Pongratz, J., van der Werf, G.R., DeFries, R.S., Hansen, M.C., Le Quéré, C., Ramankutty, N., 2012. Carbon emissions from land use and land-cover change. Biogeosciences 9, 5125–5142. https://doi.org/10.5194/bg-9-5125-2012.

Huang, W., Swatantran, A., Duncanson, L., Johnson, K., Watkinson, D., Dolan, K., O'Neil-Dunne, J., Hurtt, G., Dubayah, R., 2017. County-scale biomass map comparison: a case study for Sonoma, California. Carbon Manag 8, 417–434. https://doi.org/10.1080/17583004.2017.1396840.

Labriere, N., Tao, S., Chave, J., Scipal, K., Toan, T.L., Abernethy, K., Alonso, A., Barbier, N., Bissiengou, P., Casal, T., Davies, S.J., Ferraz, A., Herault, B., Jaouen, G., Jeffery, K.J., Kenfack, D., Korte, L., Lewis, S.L., Malhi, Y., Memiaghe, H.R., Poulsen, J.R., Rejou-Mechain, M., Villard, L., Vincent, G., White, L.J.T., Saatchi, S., 2018. In situ reference datasets from the Tropi SAR and AfriSAR campaigns in support of upcoming spaceborne biomass missions. IEEE J. Sel. Top. Appl. Earth Obs. Remote Sens. 1–11. https://doi.org/10.1109/JSTARS.2018.2851606.

Le Quéré, C., Andrew, R.M., Friedlingstein, P., Sitch, S., Pongratz, J., Manning, A.C., Korsbakken, J.I., Peters, G.P., Canadell, J.G., Jackson, R.B., Boden, T.A., Tans, P.P., Andrews, O.D., Arora, V.K., Bakker, D.C.E., Barbero, L., Becker, M., Betts, R.A., Bopp, L., Chevallier, F., Chini, L.P., Ciais, P., Cosca, C.E., Cross, J., Currie, K., Gasser, T., Harris, I., Hauck, J., Haverd, V., Houghton, R.A., Hunt, C.W., Hurtt, G., Ilyina, T., Jain, A.K., Kato, E., Kautz, M., Keeling, R.F., Klein Goldewijk, K., Körtzinger, A., Landschützer, P., Lefèvre, N., Lenton, A., Lienert, S., Lima, I., Lombardozzi, D., Metzl, N., Millero, F., Monteiro, P.M.S., Munro, D.R., Nabel, J.E.M.S., Nakaoka, S., Nojiri, Y., Padín, X.A., Peregon, A., Pfeil, B., Pierrot, D., Poulter, B., Rehder, G., Reimer, J., Rödenbeck, C., Schwinger, J., Séférian, R., Skjelvan, I., Stocker, B.D., Tian, H., Tilbrook, B., van der Laan-Luijkx, I.T., van der Werf, G.R., van Heuven, S., Viovy, N., Vuichard, N., Walker, A.P., Watson, A.J., Wiltshire, A.J., Zaehle, S., Zhu, D., 2017. Global carbon budget 2017. Earth Syst. Sci. Data Discuss 1–79. https://doi.org/10.5194/essd-2017-123.

Luckman, A., Baker, J., Honzak, M., Lucas, R., 1998. Tropical forest biomass density estimation using JERS-1 SAR: seasonal variation, confidence limits, and application to image mosaics. Remote Sens. Environ. 63, 126–139.

Magruder, L.A., Brunt, K., Alonzo, M., 2020. ICESat-2 horizontal geolocation accuracy validation using ground-based corner cube retro-reflectors. In: IEEE Transactions on Geoscience and Remote Sensing, TGRS-2019-01754, (in revision).

McRoberts, R.E., Næsset, E., Saatchi, S., Liknes, G.C., Walters, B.F., Chen, Q., 2019. Local validation of global biomass maps. Int. J. Appl. Earth Obs. Geoinf. 83 (101931).

Mitchard, E.T.A., Saatchi, S.S., Woodhouse, I.H., Nangendo, G., Ribeiro, N.S., Williams, M., Ryan, C.M., Lewis, S.L., Feldpausch, T.R., Meir, P., 2009. Using satellite radar backscatter to predict above-ground woody biomass: a consistent relationship across four different African landscapes. Geophys. Res. Lett. 36. https://doi.org/10.1029/2009GL040692.

Neuenschwander, A., Magruder, L., 2016. The potential impact of vertical sampling uncertainty on ICESat-2/ATLAS terrain and canopy height retrievals for multiple ecosystems. Remote Sens. 8, 1039. https://doi.org/10.3390/rs8121039.

Neuenschwander, A., Pitts, K., 2019. The ATL08 land and vegetation product for the ICESat-2 mission. Remote Sens. Environ. 221, 247–259. https://doi.org/10.1016/j.rse.2018.11.005.

Pan, Y., Birdsey, R.A., Houghton, R., Kauppi, P., Kurz, W., Phillips, O.L., Shvidenko, A., Lewis, S.L., Canadell, J.G., Ciais, P., Jackson, R.B., Pacala, S.W., McGuire, D.A., Piao, S., Rautiainen, A., Sitch, S., Hayes, D., 2011. A large and persistent carbon sink in the world's forests. Science 333, 984–988. https://doi.org/10.1126/science.1204588.

Pan, Y., Birdsey, R.A., Phillips, O.L., Jackson, R.B., 2013. The structure, distribution, and biomass of the world's forests. Annu. Rev. Ecol. Evol. Syst. 44, 593–622. https://doi.org/10.1146/annurev-ecolsys-110512-135914.

Patterson, P.L., Healey, S.P., Ståhl, G., Saarela, S., Holm, S., Andersen, H.-E., Dubayah, R.O., Duncanson, L., Hancock, S., Armston, J., Kellner, J.R., Cohen, W.B., Yang, Z., 2019. Statistical properties of hybrid estimators proposed for GEDI—NASA's global ecosystem dynamics investigation. Environ. Res. Lett. 14, 065007. https://doi.org/10.1088/1748-9326/ab18df.

Réjou-Méchain, M., Barbier, N., Couteron, P., Ploton, P., Vincent, G., Herold, M., Mermoz, S., Saatchi, S., Chave, J., de Boissieu, F., Féret, J.-B., Takoudjou, S.M., Pélissier, R., 2019. Upscaling forest biomass from field to satellite measurements: sources of errors and ways to reduce them. Surv. Geophys. 40, 881–911. https://doi.org/10.1007/s10712-019-09532-0.

Rosen, P., Hensley, S., Shaffer, S., Edelstein, W., Kim, Y., Kumar, R., Misra, T., Bhan, R., Satish, R., Sagi, R., 2016. An update on the NASA-ISRO dual-frequency DBF SAR (NISAR) mission. In: 2016 IEEE International Geoscience and Remote Sensing Symposium (IGARSS). IEEE, Beijing, China, pp. 2106–2108. https://doi.org/10.1109/IGARSS.2016.7729543. Presented at the IGARSS 2016-2016 IEEE International Geoscience and Remote Sensing Symposium.

Saatchi, S.S., Harris, N.L., Brown, S., Lefsky, M., Mitchard, E.T., Salas, W., Zutta, B.R., Buermann, W., Lewis, S.L., Hagen, S., et al., 2011. Benchmark map of forest carbon stocks in tropical regions across three continents. Proc. Natl. Acad. Sci. 108, 9899–9904.

Simard, M., Riel, B.V., Denbina, M., Hensley, S., 2016. Radiometric correction of airborne radar images over forested terrain with topography. IEEE Trans. Geosci. Remote Sens. 54, 4488–4500. https://doi.org/10.1109/TGRS.2016.2543142.

Yu, Y., Saatchi, S., 2016. Sensitivity of L-band SAR backscatter to aboveground biomass of global forests. Remote Sens. 8, 522. https://doi.org/10.3390/rs8060522.

Zolkos, S.G., Goetz, S.J., Dubayah, R., 2013. A meta-analysis of terrestrial aboveground biomass estimation using lidar remote sensing. Remote Sens. Environ. 128, 289–298. https://doi.org/10.1016/j.rse.2012.10.017.

Zscheischler, J., Mahecha, M.D., Avitabile, V., Calle, L., Carvalhais, N., Ciais, P., Gans, F., Gruber, N., Hartmann, J., Herold, M., 2017. Reviews and syntheses: an empirical spatiotemporal description of the global surface-atmosphere carbon fluxes: opportunities and data limitations. Biogeosciences 14, 3685–3703.